

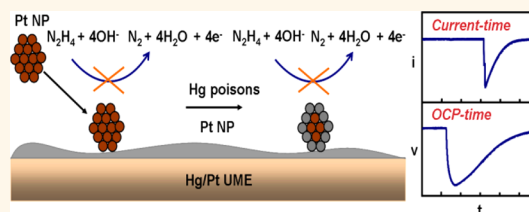
Electrochemical Monitoring of Single Nanoparticle Collisions at Mercury-Modified Platinum Ultramicroelectrodes

Radhika Dasari, Kevin Tai, Donald A. Robinson, and Keith J. Stevenson*

Department of Chemistry, The University of Texas at Austin, 1 University Station, Austin, Texas 78712, United States

ABSTRACT Here, we report a potentiometric method for detecting single platinum nanoparticles (Pt NPs) by measuring a change in open-circuit potential (OCP) instead of the current during single Pt NP collisions with the mercury-modified Pt ultramicroelectrode (Hg/Pt UME). Similar to the current–time ($i-t$) response reported previously at Hg/Pt UMEs, the OCP–time ($v-t$) response consists of repeated potential transient signals that return to the background level. This is

because Hg poisons the Pt NP after collision with the Hg/Pt UME due to amalgamation and results in deactivation of the redox reaction. For individual Pt NP collisions the amplitude of the OCP signal reaches a maximum and decays to the background level at a slower rate compared to the comparable $i-t$ response. Due to this, OCP events are broader and more symmetrical in shape compared to $i-t$ “spikes.” The collision frequency of Pt NPs derived from $v-t$ plots (0.007 to 0.020 $\text{pM}^{-1} \text{s}^{-1}$) is in good agreement with the value derived from $i-t$ plots recorded at Hg/Pt UMEs (0.016 to 0.024 $\text{pM}^{-1} \text{s}^{-1}$) under similar conditions and was found to scale linearly with Pt NP concentration. Similar to the current response, the amplitude of the OCP response increased with the NP's size. However, unlike the change in current in a $i-t$ response, the change in OCP in a $v-t$ response observed during single Pt NP collisions with Hg/Pt UME is larger than the estimated change in OCP based on the theory. Therefore, the Pt NP sizes derived from the $v-t$ response did not correlate with the TEM-derived Pt NP sizes. In spite of these results the potentiometric method has great value for electroanalysis because of its significant advantages over the amperometric method such as a simpler apparatus and higher sensitivity.



because Hg poisons the Pt NP after collision with the Hg/Pt UME due to amalgamation and results in deactivation of the redox reaction. For individual Pt NP collisions the amplitude of the OCP signal reaches a maximum and decays to the background level at a slower rate compared to the comparable $i-t$ response. Due to this, OCP events are broader and more symmetrical in shape compared to $i-t$ “spikes.” The collision frequency of Pt NPs derived from $v-t$ plots (0.007 to 0.020 $\text{pM}^{-1} \text{s}^{-1}$) is in good agreement with the value derived from $i-t$ plots recorded at Hg/Pt UMEs (0.016 to 0.024 $\text{pM}^{-1} \text{s}^{-1}$) under similar conditions and was found to scale linearly with Pt NP concentration. Similar to the current response, the amplitude of the OCP response increased with the NP's size. However, unlike the change in current in a $i-t$ response, the change in OCP in a $v-t$ response observed during single Pt NP collisions with Hg/Pt UME is larger than the estimated change in OCP based on the theory. Therefore, the Pt NP sizes derived from the $v-t$ response did not correlate with the TEM-derived Pt NP sizes. In spite of these results the potentiometric method has great value for electroanalysis because of its significant advantages over the amperometric method such as a simpler apparatus and higher sensitivity.

KEYWORDS: single nanoparticle collisions · open-circuit potential · mixed potential concept · mercury-modified Pt UMEs

Increasing interest in nanoparticles (NPs) due to their unique properties and multifarious applications has necessitated the development of new analytical tools for characterizing NPs in a fast and reproducible manner. In order to better understand the fundamental properties, correlate structure–function relationships of NPs, and optimize NP activity for various applications, it is important to probe single NPs. Hence, electroanalytical tools for detecting and characterizing individual NPs in a colloidal dispersion have been developed.^{1–17}

Compton's group detected single NPs in solution by measuring charge transfer due to electrodeposition of metals on the surface of the NP,^{1,2} electrodisolution of the NP,^{3,4} and electroreduction of redox-active ligands immobilized on the metal NP⁵ during NPs' interaction with the electrode. Bard and co-workers developed an innovative method termed “electrocatalytic amplification” for detecting single NP collision events with a ultramicroelectrode

(UME).^{6–9} In this approach, a single NP is detected by measuring charge transfer due to the electrocatalytic reaction that occurs on the surface of the NP upon its impact with an inert UME, which otherwise cannot catalyze the electrochemical reaction of interest.^{6–9} Compared to other electrochemical methods for single NP detection, this method offers great improvement in measurement sensitivity because of the continued electron flow involved with the electrocatalytic reaction. Also, general applicability of the electrocatalytic amplification method for single NP detection was demonstrated by exploring various combinations of electrode materials (Au, Pt, Pt–PtO_x, C, and B doped diamond electrode), NPs (Pt, Au, and IrO_x), and redox indicator reactions (N₂H₄, water (OH[−]), H⁺, H₂O₂, and BH₄[−]).^{6–9} Among the above-mentioned combinations, hydrazine oxidation with citrate-capped Pt NPs at Au UMEs resulted in distinguishable and reproducible catalytic responses in certain pH conditions.⁷ Utilizing

* Address correspondence to stevenson@cm.utexas.edu.

Received for review January 3, 2014 and accepted April 7, 2014.

Published online April 07, 2014
10.1021/nn500045m

© 2014 American Chemical Society

these experimental conditions (hydrazine oxidation, citrate-capped Pt NPs) we further optimized the electrocatalytic amplification method for single NP detection by replacing Au UMEs with Hg/Pt UMEs as an electrode material.^{10,11} Single Pt NP collisions with a Hg/Pt UME resulted in a reversible “spike”-shaped current–time ($i-t$) response as opposed to an irreversible “step-like” $i-t$ response at a Au UME under similar conditions.^{10,11} Additionally, compared to Au UMEs the background current observed at Hg/Pt UMEs is 2 orders of magnitude lower, which resulted in an improved signal-to-noise (S/N) ratio at Hg/Pt UMEs for ultrasensitive detection of individual NP collisions. The use of Hg/Pt UMEs also led to a reduction in surface-induced NP aggregation and electrode-fouling processes, making the measurements more reproducible and repeatable for routine detection of catalytic NPs. Unwin and co-workers recently reported a versatile pipet-based approach employing scanning electrochemical cell microscopy (SECM) for studying the reactivity of single NPs.¹⁵ However, all the above-mentioned approaches are based on measuring a change in current with time at a constant potential bias during NPs' interaction with the UME. While amperometric measurements are common for electroanalysis, potentiometric methods can offer several advantages over amperometric methods such as a simpler measurement apparatus and higher detection sensitivity.

Accordingly, Bard and co-workers recently reported a potentiometric method for detecting single Pt NPs by measuring the change in open-circuit potential (OCP) during single Pt NP collisions with the Au UME in a solution that does not contain a reversible redox species.¹⁶ The OCP of a working electrode is the value of its potential measured vs a standard reference electrode when no external current flows.¹⁶ In the presence of a reversible redox species in the solution, the OCP or the true equilibrium potential where the external current is zero is established or kinetically controlled by the two half-reactions of the same redox couple,¹⁶ whereas in the absence of the reversible redox species in the solution the equilibrium potential is determined or kinetically controlled by two or more half-reactions, a so-called *mixed potential*. The mixed potential concept was first introduced by Wagner and Traud.¹⁸ Since then this mixed potential concept has been extensively utilized for understanding several processes such as corrosion,^{19,20} poisoning affect of As species on Pt electrodes,²¹ or the deposition of Cu on a Si wafer.²² Also, gas sensors based on the mixed potential concept were developed for detecting H₂,²³ O₂,²⁴ NO_x (NO₂, N₂O, NO),²⁵ and NH₃.²⁶ However, Bard and co-workers were the first to develop a method based on the mixed potential concept for detecting single Pt NP collision events with the Au UME using hydrazine oxidation as a redox indicator reaction.¹² Further, Bard and co-workers investigated the principle involved in the potentiometric method for single NP

detection by monitoring the change in OCP when two metal electrodes (Au UME, Pt nanoelectrode) were brought into contact in a solution that contains hydrazine (irreversible redox couple).¹⁷ OCP changes in the form of a sequence of small mV steps were observed both during single Pt NP collisions with the Au UME and while the Pt nanoelectrode was in contact with the Au UME.^{16,17} This potentiometric method appeared to be more sensitive than the amperometric method for detecting single Pt NPs that are less than a few nanometers in size (*ca.* 5 nm).^{16,17} Here, we describe a potentiometric method based on the mixed potential concept for observing single NP collision events with the Hg/Pt UME through electrocatalytic amplification utilizing similar conditions to those reported in the literature.¹⁶ This newly developed method has the added advantage of highly sensitive potentiometric detection of single NP collisions with Hg/Pt UMEs in a reliable and repeatable manner. This improved detection sensitivity in turn enables the detection of NPs that are less than a few nanometers at an ultratrace concentration (<μM) of redox indicator reactions (*e.g.*, hydrazine oxidation and proton reduction).

RESULTS AND DISCUSSION

Compared with Hg, Pt is a better electrocatalyst for hydrazine oxidation. The difference in the onset potential for hydrazine oxidation at Pt and Hg UME in 15 mM hydrazine in 50 mM phosphate buffer of pH ~7.5 is *ca.* -0.38 V (see Figure S1), whereas the difference in the mixed OCP of Hg/Pt UME and Pt UME in 15 mM hydrazine solution in 50 mM phosphate buffer of pH ~7.5 is ~0.34 V, as shown in Figure 1A. Here, the mixed OCP is determined by hydrazine oxidation and proton reduction and is possibly due to the reduction of trace amounts of oxygen. The OCP of Hg/Pt UME and Pt UME in 15 mM hydrazine in 50 mM phosphate buffer of pH ~7.5 is -0.04 and -0.38 V vs a Ag/AgCl reference electrode, respectively. The OCP at these electrodes decreases very slowly, remaining essentially constant with time. Figure 1B shows the OCP–time ($v-t$) plot at Hg/Pt UME after injection of Pt NPs in 15 mM hydrazine and 50 mM phosphate buffer at pH ~7.5. A very distinct change in the OCP in the form of “spikes” that are much larger than the baseline noise level (100 μV) can be seen after injecting Pt NPs into a hydrazine solution, whereas in a control experiment, where Pt NPs were introduced in 50 mM phosphate buffer at pH ~7.5 in the absence of hydrazine, no distinct change in OCP was observed, as shown in Figure 1C. This response clearly indicates that the OCP “spikes” observed after injecting Pt NPs in hydrazine solution are indeed due to the hydrazine oxidation catalyzed by Pt NP during its interaction with the Hg/Pt UME. Also, we note that current transients in the form of “spikes” were observed while measuring the current at a constant potential bias at Hg/Pt UME under similar

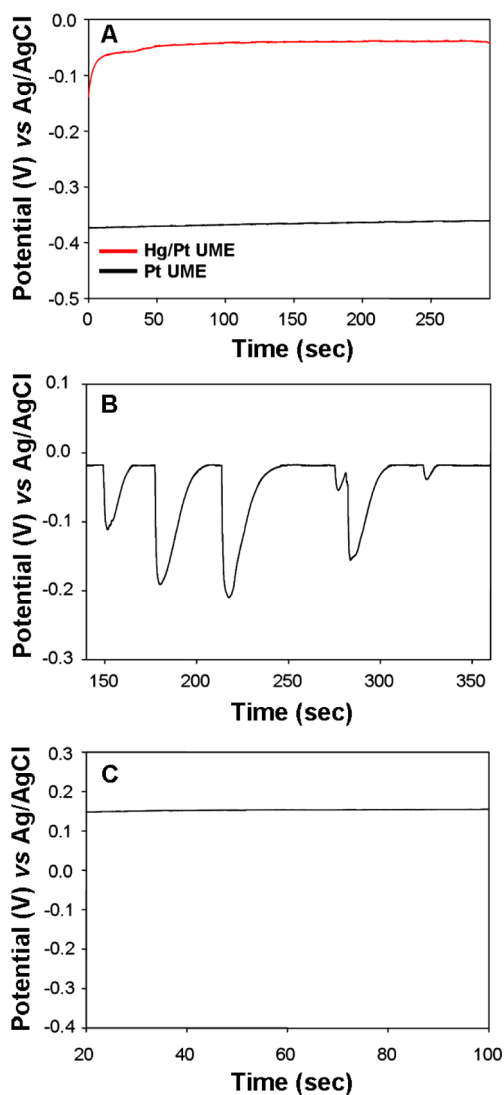


Figure 1. (A) OCP vs time plot of Hg/Pt (radius $\sim 12.5 \mu\text{m}$) and Pt UMEs (radius $\sim 12.5 \mu\text{m}$) in a solution of 15 mM hydrazine in 50 mM phosphate buffer at pH ~ 7.5 . The OCP vs time curve after injecting Pt NPs in (B) 15 mM hydrazine in 50 mM phosphate buffer of pH ~ 7.5 and (C) 50 mM phosphate buffer of pH ~ 7.5 in the absence of hydrazine [data acquisition interval (t_{data}), 1.5 ms; NP size, $\sim 4.2 \text{ nm}$; NP concentration, $\sim 2 \text{ pM}$].

conditions.^{10,11} In stark contrast, the $i-t$ and $v-t$ transients observed for single Pt NP collisions with Au UMEs under similar conditions are both in the form of “steps”.^{6–8} “Spike”-shaped current transients at Hg/Pt UME have been ascribed to the deactivation of Pt NPs due to amalgamation after the NPs are stuck to the Hg/Pt UME following a collision.²⁷ However, in the case of Au UMEs, Pt NPs retain their catalytic activity after sticking to the electrode, which leads to an irreversible change in current or OCP.^{6–8,16,17}

The fundamental principle involved in observing a change in OCP after a Pt NP collision event with the Hg/Pt UME is illustrated schematically with current–potential ($i-E$) curves in Figure 2. Once the Pt NP contacts the Hg/Pt UME or is at a distance where electrons

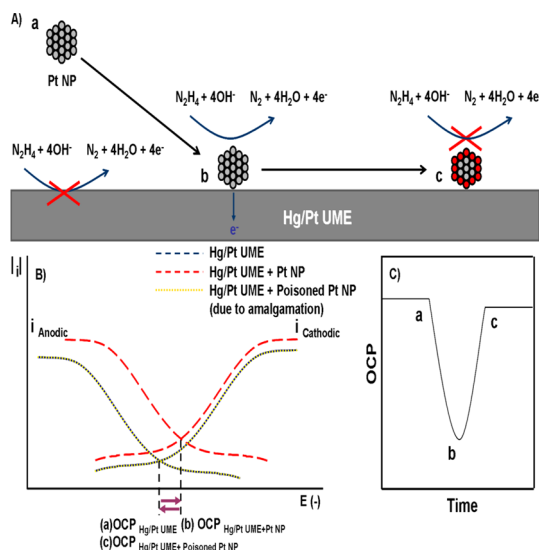


Figure 2. Schematic representation of the (A) principle involved in monitoring single Pt NP collision events at a Hg/Pt UME, (B) half-reaction $i-E$ curves before and after a single Pt NP collision event on the Hg/Pt UME, (C) OCP change caused by electrocatalytic hydrazine oxidation.

can tunnel between the Pt NP and the Hg/Pt UME, the Pt NP electrocatalyzes the hydrazine oxidation and the overall oxidation current (current on the Pt NP combined with the Hg/Pt UME) becomes larger than the overall reduction current. To maintain the OCP condition, the potential shifts to a more negative value to produce a zero net current. However, once the Pt NP interacts with the Hg/Pt UME, Hg poisons the Pt NP due to amalgamation, deactivates the redox reaction, and eventually turns off the catalytic reaction. As a result, the overall oxidation current (current on the Pt NP combined with Hg/Pt UME) becomes smaller than the overall reduction current. Again, to maintain the OCP condition, the potential now shifts to a more positive value to produce a net zero current. Hence, at the Hg/Pt UME, the $v-t$ response is in the form of a sequence of few millivolt “spikes” as opposed to “steps” at Au UMEs under similar conditions.

In order to confirm that the observed OCP transients are due to individual Pt NPs, single Pt NP collision experiments with Hg/Pt UMEs were performed in 15 mM hydrazine solution containing different concentrations of Pt NPs. As shown in Figure 3, the number of OCP transients increased with an increase in Pt NP concentration, indicating that the observed OCP transients after injecting Pt NPs are due to individual Pt NPs. Also, the collision frequency determined from $v-t$ plots was found to be $0.007\text{--}0.02 \text{ pM}^{-1} \text{ s}^{-1}$. This value is in good agreement with the collision frequency obtained from $i-t$ plots recorded at Hg/Pt UMEs ($0.016\text{--}0.024 \text{ pM}^{-1} \text{ s}^{-1}$)¹⁰ and Au UMEs ($0.012\text{--}0.02 \text{ pM}^{-1} \text{ s}^{-1}$)⁷ under similar conditions. However, we note that if all the NPs that collide with the UME lead to a change in current or OCP in a $i-t$ and $v-t$ response recorded during single Pt NP collisions, then

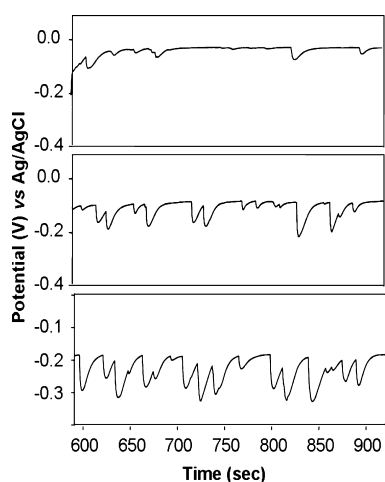


Figure 3. (A) OCP vs time plots for single Pt NP collisions at Hg/Pt UME (radius $\sim 12.5 \mu\text{m}$) in 15 mM hydrazine + 50 mM phosphate buffer pH ~ 7.5 solution containing various concentrations of Pt NPs, 1–4 pM [data acquisition interval (t_{data}), 1.5 ms; NP size, ~ 4.2 nm].

the NP diffusion coefficient estimated from the collision frequency observed experimentally should match with the diffusion coefficient estimated from Stokes–Einstein relation. However, these estimations do not agree. The collision frequency of 3–4 nm Pt NPs determined experimentally from $i-t$ and $v-t$ plots is in the range $0.0007\text{--}0.024 \text{ pM}^{-1} \text{ s}^{-1}$.^{10,11} This value corresponds to a diffusion coefficient of $2 \times 10^{-8} \text{ cm}^2/\text{s}$. This value is lower than the diffusion coefficient estimated for 3–4 nm Pt NPs using the Stokes–Einstein relation, which is $1 \times 10^{-8} \text{ cm}^2/\text{s}$. This suggests that not all the NPs that collide with the UME lead to a change in current or OCP in a $i-t$, $v-t$ response recorded during single Pt NP collisions with the Hg/Pt UME. Rather, only NPs that stick to the UME might lead to a change in current or OCP in a $i-t$ and $v-t$ response recorded during single Pt NP collisions with the Hg/Pt UME. The observed frequency more likely is a sticking probability than the collision frequency. Another trend observed in the case of amperometric measurements was an increase in the amplitude of the current “spike” with respect to Pt NP size at constant NP and hydrazine concentration.¹⁰ Therefore, one would also expect to observe an increase in amplitude of the OCP response with an increase in Pt NP size at constant NP and hydrazine concentration if the observed $v-t$ transients are due to individual Pt NP collisions with Hg/Pt UME. Accordingly, single Pt NP collision experiments were performed with two samples of Pt colloidal solution of different particle sizes synthesized using the procedure reported before.²⁸ The average sizes of the NPs were determined to be 4 ± 1 and 23 ± 8 nm from the TEM images and respective histograms shown in Figure S2. Figure S3A,B show representative $v-t$ plots recorded for the corresponding Pt NPs shown in Figure S2A,B. The $v-t$ plots recorded with Pt colloidal solutions of different particle sizes showed discrete

OCP events of different amplitude. Any difference in the OCP events is due to differences in NP size and size polydispersity since all the other parameters except the size of the Pt NPs were kept constant. With an increase in Pt NP size, the amplitude of the OCP response increased. For larger Pt NPs, sequences of OCP events of integrated potential were concentrated over a range of 20 to 80 mV, whereas for the smaller Pt NPs the integrated potential under an OCP event was concentrated over a range of 5 to 30 mV. This measurement confirms that the observed OCP events after injecting Pt NPs in hydrazine solution are due to individual Pt NP collisions. Also, this measurement suggests that the potentiometric method can be used for differentiating NPs of different sizes based on their catalytic activity.

In order to compare the potentiometric method with the previously reported amperometric method for sizing Pt NPs, we obtained both $i-t$ and $v-t$ plots at the same Hg/Pt UME using aliquots of 4.2 nm Pt NPs from the same batch of Pt NP colloidal solution. We note that instrumental limitations such as sampling interval can influence the nature of the current or OCP response observed during single Pt NP collisions with the Hg/Pt UME. Hence, to rule out the influence of sampling interval on the nature of the current or OCP response observed during single Pt NP collisions with the Hg/Pt UME, we used a sampling interval of ~ 1.5 ms while performing both the amperometric and potentiometric measurements. Figure 4A,B show $i-t$ and $v-t$ plots recorded consecutively at the same Hg/Pt UME after injecting 4.2 nm Pt NPs in 15 mM hydrazine in 50 mM phosphate buffer solution of pH ~ 7.5 . Although “spike”-shaped transients were observed while measuring OCP or current with time, OCP transients are distinctly different from the current transients. At an individual OCP event the potential reaches a maximum amplitude and then decays to the background level at a slower rate compared to a current “spike” (see Figure 5). On average, at an individual OCP event the potential reaches the maximum amplitude in ~ 2.77 s and decays to the background level in ~ 10.4 s compared to ~ 0.64 and ~ 2.13 s, respectively, for current in a current “spike”. As a result, OCP transients appear more symmetrical (broader) in shape compared to current transients and are in the form of “peaks”. Several factors could be responsible for the observation of broader OCP transients. For example, in general, establishment of an equilibrium potential where the net current is zero could be slow in potentiometric measurements. Also, Pt NPs are deactivated due to amalgamation after sticking to the Hg/Pt UME. Therefore, the amalgamation process is at play along with the two half-reactions in the case of Hg/Pt UMEs. Hence, the amalgamation process might influence the establishment of an equilibrium potential. The amount of electrocatalytic current generated due to both half-reactions is determined by the catalytically

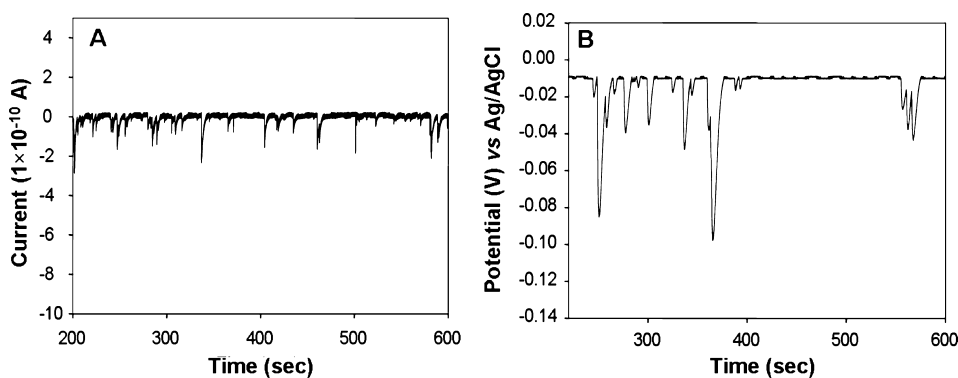


Figure 4. (A) Current vs time and (B) OCP vs time plots for single Pt NP collisions at the Hg/Pt UME (radius $\sim 12.5 \mu\text{m}$) in the presence of 50 mM phosphate buffer (pH 7.5) and 15 mM hydrazine with 1 pM Pt NPs [data acquisition interval (t_{data}), 1.5 ms; NP size, $\sim 4.2 \text{ nm}$; NP concentration, $\sim 6 \text{ pM}$].

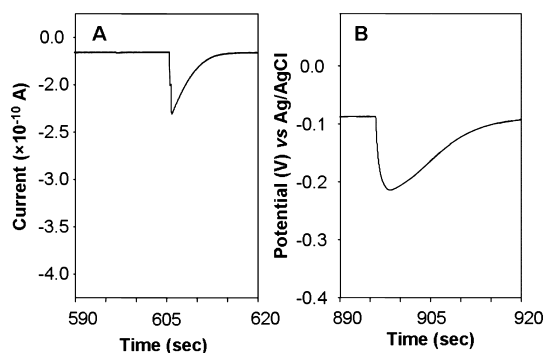


Figure 5. (A) Current vs time and (B) OCP vs time plots for single Pt NP collisions at the Hg/Pt UME (radius $\sim 12.5 \mu\text{m}$) in the presence of 50 mM phosphate buffer (pH 7.5) and 15 mM hydrazine with 1 pM Pt NPs [data acquisition interval (t_{data}), 1.5 ms; NP size, $\sim 22.9 \text{ nm}$; NP concentration, $\sim 2 \text{ pM}$].

active surface area of the Pt NP which in turn is determined by the Pt NP surface area that is amalgamated (deactivated). For this reason, the rate at which the amalgamation process occurs or, in other words, how quickly a Pt NP is completely deactivated might determine the pulse width of the $v-t$ response. Other factors such as perturbation of hydrazine concentration and the product diffusion being felt over a wide range of the substrate area could also influence the establishment of the equilibrium potential.

As reported before,¹² we estimated the Pt NP size distribution from the $i-t$ plots using the equation for calculating the amplitude of current at the mass transfer limiting current generated at an individual spherical metal NP in contact with a planar electrode. The integrated charge passed per $i-t$ "spike" during a single collision event concentrated over a range of 15–75 pA (see Figure 6A). As shown in Figure S4, the average size determined from the $i-t$ plot ($4.1 \pm 1.5 \text{ nm}$) correlated well with theory and the TEM-derived average size ($4.2 \pm 1.3 \text{ nm}$). Further, to test whether the change in OCP observed during single Pt NP collisions with the Hg/Pt UME correlates with the previously formulated theory and TEM-derived sizes, $i-E$ curves were simulated using the equations

reported before for estimating half-reaction currents.¹⁷ Both the simulated anodic current (i_A) and cathodic current (i_C) vs potential (E) plots were constructed for a $12.5 \mu\text{m}$ Hg/Pt UME and a 4.2 nm Pt NP (Figure 7). Also included is the overall (Hg/Pt UME + Pt NP) i_A and i_C when the Pt NP is in contact with the Hg/Pt UME. The equations used for estimating the half-reaction currents are as follows:

$$i_C = (K_C^\circ/m_O)i_{dc} \exp[-\alpha'_C f(E - E_C^\circ)]$$

$$i_A = (K_A^\circ/m_R)i_{dA} \exp[(1 - \alpha'_A)f(E - E_A^\circ)]$$

where K_C° and K_A° are the rate constants, E_C° and E_A° are the assumed standard potentials of the overall half-reactions, i_{dc} and i_{dA} are the mass transfer limiting currents, m_O and m_R are the mass transfer coefficients, α'_C and α'_A are the charge transfer coefficients, and $f = F/RT$. Table S1 shows the parameters used for generating $i-E$ curves.

The following assumptions are made while generating the $i-E$ curves: (1) the potential of the electrode is controlled by single half cathodic reaction current, e.g., for proton or water reduction ($2\text{H}^+ \rightarrow \text{H}_2 + 2\text{e}^-$), and a single half anodic reaction current, e.g., for hydrazine oxidation ($\text{N}_2\text{H}_4 \rightarrow \text{N}_2 + 4\text{H}^+ + 4\text{e}^-$); (2) the anodic reaction rate constant of Hg is similar to the anodic reaction rate constant of Au. We note that, since the anodic reaction rate constant of Hg (K_A° of Hg) cannot be determined, the anodic reaction rate constant of Au (K_A° of Au) is used instead in the calculations. Further, the cyclic voltammograms of hydrazine oxidation at Hg/Pt UMEs and Au UMEs show that onset potential for hydrazine oxidation at both these electrodes are similar (see Figure S1), which indicates the assumption is appropriate. Figure 7 shows a simulated series of i_A and i_C vs E plots of Hg/Pt UME, Pt NP, and overall (Hg/Pt UME + Pt NP) anodic and cathodic current when Pt NP is in contact with the Hg/Pt UME. The intersection point of the $i-E$ plot indicates the OCP where the net current equals zero ($i_A = i_C$). The estimated change in OCP when a 4.2 nm Pt NP contacted

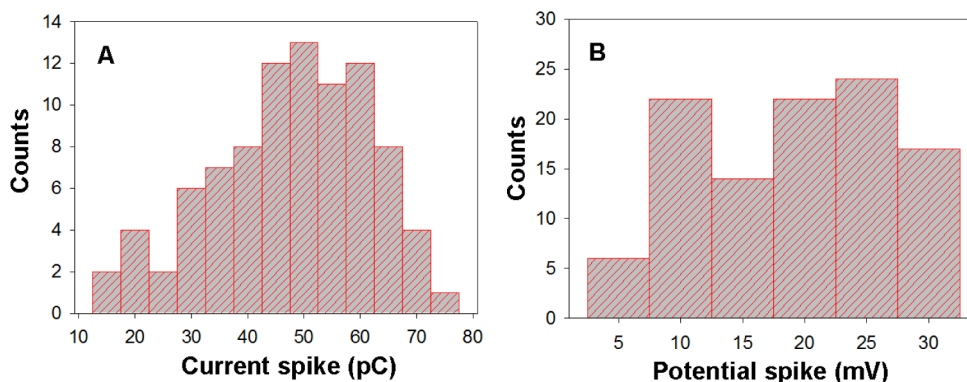


Figure 6. Histograms showing the statistical distribution of all recognizable (A) potential spikes and (B) current spikes of different amplitudes at the NP concentration of ~ 1 pM.

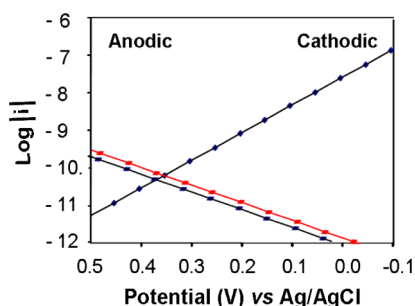


Figure 7. Simulated i - E plots of anodic and cathodic current vs potential plot of Hg/Pt UME (blue) and Hg/Pt UME + Pt NP (red) generated based on theory.

the $12.5 \mu\text{m}$ Hg/Pt UME is 8 mV. Also, as in the case of i - t plots, the potential under the OCP spike was integrated to determine the change in OCP observed during single Pt NP collisions with the Hg/Pt UMEs. The integrated potential under an OCP spike concentrated over a range of 5 to 30 mV (see Figure 6B). The change in OCP observed during single Pt NP collisions with Hg/Pt UME is larger than the estimated change based on the theory and does not correlate with size-dependent OCP magnitudes estimated from TEM-derived sizes. Considering the several assumptions made to generate i - E curves, a discrepancy in the change in OCP estimated based on theory with the observed change in OCP is not surprising. For instance, the standard reduction or oxidation potential is the potential in volts vs NHE generated by half-reaction at standard conditions (25°C , 1 atm, 1 M concentration), whereas the single Pt NP collision experiments were not performed under these standard conditions.

We also note that at a $5 \mu\text{m}$ Au UME with ~ 4 nm Pt NPs the change in OCP concentrated over a range of 0.5 to 2 mV during single Pt NP collisions with the electrode.¹⁶ In contrast, at a $12.5 \mu\text{m}$ Hg/Pt UME with Pt

NPs of similar size the change in OCP concentrated over a range of 5 to 30 mV. The change in OCP observed at Hg/Pt UMEs during single Pt NP collisions is 2.5 to 15 times larger than the change in OCP observed at Au UMEs. This still is an underestimation because the radius of Hg/Pt UMEs used in the experiments is larger than the Au UME. It has been reported in the literature that the magnitude of the OCP signal is heavily influenced by the ratio of electrode size to Pt NP.^{16,17} With an increase in the ratio of electrode size to Pt NP size the magnitude of an OCP event should increase. We also note that at a $12.5 \mu\text{m}$ Au UME with 4 nm Pt NPs no significant change in the OCP was observed during single NP collisions. This observation clearly indicates that utilization of Hg/Pt UMEs as a detection platform coupled with potentiometric methods has improved sensitivity for detection of single Pt NP collisions than previously reported methods in the literature.

CONCLUSIONS

In conclusion, here we have demonstrated that single Pt NP collision events using Hg/Pt UMEs can be reliably and reproducibly detected by measuring a change in OCP. Similar to the change in current, a change in OCP during single Pt NP collisions with Hg/Pt UMEs is in the form of a "spike." In contrast to current "spikes" resulting from controlled potential step experiments, OCP "spikes" are more symmetrical in shape, and the change in OCP observed during single Pt NP collisions is larger than the estimated change in OCP based on existing formulated theory. However, the sensitivity of the potentiometric method for single NP detection is increased due to the utilization of Hg/Pt UMEs as an electrode material compared to Au. These attributes in turn enable the ultrasensitive detection of NPs that are less than a few nanometers in size.

METHODS

Chemicals. Hydrazine monohydrate (64% N_2H_4 , 98%), chloroplatinic acid hydrate (H_2PtCl_6 , 99.9%), and mercury(II) nitrate

monohydrate ($\text{Hg}(\text{NO}_3)_2$, 98.0%) were purchased from Sigma-Aldrich (St. Louis, MO, USA) and used as received. The following chemicals were purchased from Fisher Scientific (Fair Lawn,

NJ, USA) and used as received: sodium phosphate monobasic monohydrate, sodium phosphate dibasic anhydrous, nitric acid (69.3% in water), hydrochloric acid (HCl, 37% in water), and acetone (99.9%, HPLC grade). The following additional chemicals were used as received: sodium borohydride (NaBH_4 , 98.0%, Acros Organics, Geel, Belgium), sodium citrate (99.0%, Alfa Aesar, Ward Hill, MA, USA), and ethanol (99.5%, anhydrous, Pharmco-AAPER, Brookfield, CT, USA). Nanopure water from a Barnstead nanopure filtration system having a resistivity of 18 $\text{M}\Omega$ cm was used for all experiments.

Synthesis of Pt Nanoparticles. Pt NPs of two different sizes were synthesized following a procedure previously reported.²⁸ Pt seed particles were synthesized by adding 6.97 mL of a 0.2% chloroplatinic acid hexahydrate solution to 89.9 mL of boiling nanopure water (resistivity of $>19 \text{ M}\Omega$ cm from a Barnstead nanopure water system). After 1 min, 2.13 mL of a solution containing 1% sodium citrate and 0.05% citric acid was added. After an additional 30 s, 1.06 mL of freshly prepared solution containing 0.08% sodium borohydride, 1% sodium citrate, and 0.05% citric acid solution was added. The solution was allowed to boil for another 10 min.

Pt NPs of larger diameter were prepared by adding 1 mL of the Pt seed solution described above to 29 mL of nanopure water at room temperature. To this was added 0.045 mL of 0.4 M chloroplatinic acid solution. To this solution was added 0.5 mL of a solution containing 1% sodium citrate and 1.25% L-ascorbic acid solution. The mixture was then heated slowly to the boiling point over a period of ~ 30 min under stirring. The solution turned dark, indicating the formation of Pt NPs. Pt NP solutions were dialyzed to remove excess salts.

Fabrication of Hg/Pt UME. Hg/Pt UMEs were fabricated by following the procedure reported before.²⁹ Hg was electroplated onto the platinum surface from a solution containing 5.7 mM mercury nitrate, 0.5% concentrated nitric acid, and 1 M potassium nitrate by holding the potential at -0.1 V vs a Ag/AgCl reference electrode for 333 s. The onset potential for H_2 evolution before and after electrodepositing Hg on the Pt surface was tested to confirm the modification of the Pt UME surface with Hg (see Figure S5).

Instrumentation. Cyclic voltammetry, chronoamperometry, and potentiometric measurements were performed with a three-electrode cell containing about 20 mL of electrolyte, controlled by an electrochemical workstation (CH Instruments, Austin, TX, USA, model 700A). Ag/AgCl was used as a reference electrode. Throughout the experiment the electrochemical cell was maintained as vibration-free as possible under a Faraday cage in an Ar environment. The current and OCP were recorded vs time before and after injecting NP solution. A sampling interval of ~ 1.5 ms and the default filter setting were used while performing both amperometric and potentiometric measurements. Also to ensure proper distribution of Pt NPs in solution, the solution was bubbled with Ar for 10 s after injecting NPs. Due to the opening and closing of the Faraday cage for injecting the NPs, noise would appear in the $i-t$ and $v-t$ plots. TEM images were acquired from a Jeol 2010F TEM operated at 200 kV.

Conflict of Interest: The authors declare no competing financial interest.

Acknowledgment. We gratefully acknowledge the DTRA (grant HDTRA1-11-10005) for funding this project and Drs. Richard M. Crooks, Allen J. Bard, and Bo Zhang for valuable discussions. R.D. acknowledges Nellymar Membreno for acquiring TEM images.

Supporting Information Available: Cyclic voltammograms of hydrazine oxidation at Au, Pt, and Hg/Pt UMEs, proton reduction at a Pt UME and Hg/Pt UME, TEM images of Pt NPs, histograms showing the size distribution of Pt NPs, $v-t$ and $i-t$ plots showing single Pt NP collisions of different size Pt NPs with a Hg/Pt UME, and table showing the parameters used for generating $i-E$ curves. This material is available free of charge via the Internet at <http://pubs.acs.org>.

REFERENCES AND NOTES

- Zhou, Y.-G.; Rees, N. V.; Compton, R. G. Nanoparticle–Electrode Collision Processes: The Electroplating of Bulk Cadmium on Impacting Silver Nanoparticles. *Chem. Phys. Lett.* **2011**, *511*, 183–186.
- Rees, N. V.; Zhou, Y.-G.; Compton, R. G. Nanoparticle–Electrode Collision Processes: The Underpotential Deposition of Thallium on Silver Nanoparticles in Aqueous Solution. *ChemPhysChem* **2011**, *12*, 2085–2087.
- Zhou, Y.-G.; Rees, N. V.; Pillay, J.; Tshikhudo, R.; Vilakazi, S.; Compton, R. G. Gold Nanoparticles Show Electroactivity: Counting and Sorting Nanoparticles upon Impact with Electrodes. *Chem. Commun.* **2012**, *48*, 224–226.
- Zhou, Y.-G.; Rees, N. V.; Compton, R. G. The Electrochemical Detection and Characterization of Silver Nanoparticles in Aqueous Solution. *Angew. Chem., Int. Ed.* **2011**, *50*, 4219–4221.
- Zhou, Y.-G.; Rees, N. V.; Compton, R. G. The Electrochemical Detection of Tagged Nanoparticles via Particle–Electrode Collisions: Nanoelectroanalysis Beyond Immobilisation. *Chem. Commun.* **2012**, *48*, 2510–2512.
- Xiao, X.; Bard, A. J. Observing Single Nanoparticle Collisions at an Ultramicroelectrode by Electrocatalytic Amplification. *J. Am. Chem. Soc.* **2007**, *129*, 9610–9612.
- Xiao, X.; Fan, F.-R. F.; Zhou, J.; Bard, A. J. Current Transients in Single Nanoparticle Collision Events. *J. Am. Chem. Soc.* **2008**, *130*, 16669–16677.
- Kwon, S. J.; Zhou, H.; Bard, A. J. Electrochemistry of Single Nanoparticles via Electrocatalytic Amplification. *Isr. J. Chem.* **2010**, *50*, 267–276.
- Kwon, S. J.; Fan, F.-R. F.; Bard, A. J. Observing Iridium Oxide (IrO_x) Single Nanoparticle Collisions at Ultramicroelectrodes. *J. Am. Chem. Soc.* **2010**, *132*, 13165–13167.
- Dasari, R.; Robinson, D. A.; Stevenson, K. J. Ultrasensitive Electroanalytical Tool for Sizing, Detecting and Evaluating the Catalytic Activity of Platinum Nanoparticles. *J. Am. Chem. Soc.* **2013**, *135*, 570–573.
- Dasari, R.; Walther, B.; Robinson, D. A.; Stevenson, K. J. Influence of Redox Indicator Reaction on Single Nanoparticle Collisions at Mercury and Bismuth Modified Pt Ultramicroelectrodes. *Langmuir* **2013**, *29*, 15100–15106.
- Sardesai, N. P.; Andrescu, D.; Andrescu, S. Electroanalytical Evaluation of Antioxidant Activity of Cerium Oxide Nanoparticles by Nanoparticle Collisions at Microelectrodes. *J. Am. Chem. Soc.* **2013**, *135*, 16770–16773.
- Kleijn, S. E. F.; Serrano-Bou, B.; Yanson, A. I.; Koper, M. T. M. Influence of Hydrazine Induced Aggregation on the Electrochemical Detection of Platinum Nanoparticles. *Langmuir* **2013**, *29*, 2054–2064.
- Qiu, D.; Wang, S.; Zheng, Y.; Deng, Z. One at a Time: Counting Single-Nanoparticle/Electrode Collisions for Accurate Particle Sizing by Overcoming the Instability of Gold Nanoparticles under Electrolytic Conditions. *Nanotechnology* **2013**, *24*, 505707.
- Kleijn, S. E. F.; Lai, S. C. S.; Miller, T. S.; Yanson, A. I.; Koper, M. T. M.; Unwin, P. R. Landing and Catalytic Characterization of Individual Nanoparticles on Electrode Surfaces. *J. Am. Chem. Soc.* **2012**, *134*, 18558–18561.
- Zhou, H.; Park, J. H.; Fan, F.-R. F.; Bard, A. J. Observation of Single Metal Nanoparticle Collisions by Open Circuit (Mixed) Potential Changes at an Ultramicroelectrode. *J. Am. Chem. Soc.* **2012**, *134*, 13212–13215.
- Park, J. H.; Zhou, H.; Percival, S. J.; Zhang, Bo.; Fan, F.-R. F.; Bard, A. J. Open Circuit (Mixed) Potential Changes upon Contact between Different Inert Electrodes–Size and Kinetic Effects. *Anal. Chem.* **2012**, *85*, 964–970.
- Wagner, V. C.; Traud, W. Interpretation of Corrosion Phenomena by Superimposition of Electrochemical Partial Reaction and the Formation of Potentials of Mixed Electrodes. *Elektrochem.* **1938**, *44*, 391–402.
- Wagner, V. C.; Traud, W. On the Interpretation of Corrosion Processes through the Superposition of Electrochemical Partial Processes and on the Potential of Mixed Electrodes, with a Perspective by F. Mansfeld. *Corrosion* **2006**, *62*, 843–855.
- Zelinsky, A. G.; Pirogov, B. Ya.; Yurjev, O. A. Open Circuit Potential Transients and Electrochemical Quartz Crystal Microgravimetry Measurements of Dissolution of Copper

- in Acidic Sulfate Solutions. *Corros. Sci.* **2004**, *46*, 1083–1093.
21. Gao, I. J.; Conway, B. E. Poisoning Effects of Arsenic Species on H₂ Adsorption and Kinetic Behaviour of the H₂ Evolution Reaction at Pt in KOH Solution. *J. Electroanal. Chem.* **1995**, *395*, 261–271.
 22. Parkhutik, V.; Rayon, E.; Pastor, E.; Matveeva, E.; Sasano, J.; Ogata, Y. Study of Oscillatory Behavior of Open Circuit Potential of Silicon Immersed In CuSO₄/HF Solutions. *Phys. Status Solidi* **2005**, *202*, 1586–1591.
 23. Sekhar, P. K.; Brosha, E. L.; Mukundan, R.; Nelson, M. A.; Willaimson, T. L.; Grazon, F. H. Development and Testing of a Miniaturized Hydrogen Safety Sensor Prototype. *Sens. Actuators, B* **2010**, *148*, 469–477.
 24. Vallieres, C.; Gray, J.; Poncin, S.; Matlosz, M. Potentiometric Detection of Oxygen Based on the Mixed Potential of Zinc. *Electroanalysis* **1998**, *10*, 191–197.
 25. Lu, G.; Miura, N.; Yamazoe, N. High-Temperature Sensors for NO and NO₂ Based on Stabilized Zirconia and Spinel-Type Oxide Electrodes. *J. Mater. Chem.* **1997**, *7*, 1445–1449.
 26. Schonauer, D.; Wiesner, K.; Fleischer, M.; Moos, R. Selective Mixed Potential Ammonia Exhaust Gas Sensor. *Sens. Actuators, B* **2009**, *140*, 585–590.
 27. Whitesides, G. M.; Hackett, M.; Brainard, R. L.; Lavalleye, J. P. P. M.; Sowinski, A. F.; Izumi, A. N.; Moore, S. S.; Brown, D. W.; Staudt, E. M. Suppression of Unwanted Heterogeneous Platinum(0)-Catalyzed Reactions by Poisoning with Mercury(0) in Systems Involving Competing Homogeneous Reactions of Soluble Organoplatinum Compounds: Thermal Decomposition of Bis(triethylphosphine)-3,3,4,4-tetramethylplatinacyclopentane. *Organometallics* **1985**, *4*, 1819–1830.
 28. Bigall, N. C.; Härtling, T.; Klose, M.; Simon, P.; Eng, L. M.; Eychmüller, A. Monodisperse Platinum Nanospheres with Adjustable Diameters from 10 to 100 nm: Synthesis and Distinct Optical Properties. *Nano Lett.* **2008**, *8*, 4588–4592.
 29. Wehmeyer, K. R.; Wightman, M. Cyclic Voltammetry and Anodic Stripping Voltammetry with Mercury Ultramicroelectrodes. *Anal. Chem.* **1985**, *57*, 1989–1993.